coatings

MDPI

Article

Synthesis and Morphological Characterization of Nanoporous Aluminum Oxide Films by Using a Single Anodization Step

Florencia Alejandra Bruera [1,2], Gustavo Raúl Kramer [1,2], María Laura Vera [1,2] and Alicia Esther Ares [1,2,*]

1 Instituto de Materiales de Misiones (IMAM), Consejo Nacional de Investigaciones Científicas y Técnicas (CONICET)-Universidad Nacional de Misiones (UNaM), Posadas 3300, Misiones, Argentina; brueraflorencia@gmail.com (F.A.B.); guskramer@gmail.com (G.R.K.); veramalau@gmail.com (M.L.V.)

2 Facultad de Ciencias Exactas, Químicas y Naturales (FCEQyN), Universidad Nacional de Misiones (UNaM), Posadas 3300, Misiones, Argentina

* Correspondence: aares@fceqyn.unam.edu.ar; Tel.: +54-376-442-2186/449-7141 (ext. 125)

Received: 14 December 2018; Accepted: 11 February 2019; Published: 13 February 2019

Abstract: Nanoporous anodic aluminum oxide (AAO) films play an important role in nanotechnology due to their easily adjustable morphological properties and wide range of applications. Thus, a deep and systematic characterization of the morphological properties of these coatings is essential. The most important variables in the synthesis of nanoporous AAO films include the anodization voltage, nature, concentration and temperature of the electrolyte, which, combined, result in pores of different sizes and geometries. In the present work, AA 1050 alloy was used to synthesize AAO films, using 0.3 and 0.9 M oxalic acid as the electrolyte and combining different electrolyte temperatures (20, 30 and 40 °C) and anodizing voltages (30, 40 and 60 V), with the aim to correlate the morphological properties of the coatings with the synthesis parameters of a single anodization step. The coatings obtained were characterized by optical microscopy and scanning electron microscopy, determining pore diameter, interpore distance, pore density and coating thickness. The results showed that, by varying the anodic synthesis conditions, it is possible to obtain coatings with a pore diameter between 21 and 97 nm, an interpore distance between 59 and 138 nm, pore density between 2.8×10^{10} and 5.4×10^{9} pores/cm^2 and thicknesses between 15 and 145 μm. In this way, the right combination of synthesis variables allows synthesizing AAO coatings with morphological characteristics best suited to each particular application.

Keywords: anodic oxidation; nanostructured coatings; AA 1050; one-step anodization

1. Introduction

Aluminum anodic oxidation is a simple, low-cost and versatile electrochemical process that allows obtaining nanoporous coatings of different morphology, by varying the electrochemical parameters of synthesis such as the nature, concentration and temperature of the electrolyte and the anodization voltage [1].

Over the years, many efforts have been made to optimize the use of nanoporous anodic aluminum oxide (AAO) films in applications such as molecular filtration and separation, catalysis, electronics and photonics, energy generation and storage, sensors and biosensors, drug delivery and template synthesis to obtain nanotubular materials [2–4]. In this sense, Masuda and Fukuda [5] developed a two-step anodization technique to obtain self-ordered nanostructures and hexagonal packaging of pores, without the need for expensive lithographic techniques [5,6], which was a breakthrough in obtaining nanomaterials from AAO templates. However, synthesis with only one anodization step for

nanotechnological applications, that do not require too much order in the network of pores, is still an alternative with lower production times and costs.

In general, most researchers studying aluminum anodization use electrolytes at low temperatures (in the range of 0–5 °C) [7–12] to reduce the high current density rates that result from oxide dissolution [13,14]. This implies very slow oxide growth rates [15], which demand many hours of anodization and increase synthesis costs. However, near ambient temperatures (equal to or greater than 20 °C) significantly shorten the anodization time, allowing the synthesis of thick membranes in a short time, without the need for a cooling circuit [3]. Another way to minimize AAO film synthesis costs is to use commercial aluminum alloys such as AA 1050 (99.5% Al) [1,16–19] as the substrate, although high-purity aluminum anodizing allows obtaining higher order films [11,15,20,21].

The objective of this work was to synthesize and characterize low-cost nanoporous coatings obtained by means of one-step anodization of the commercial alloy AA 1050 by using oxalic acid at near ambient temperatures for technological applications such as catalysis, filtration and molecular separation in which the order of the porous arrangement is not decisive. Particularly, in catalytic applications, the use of nanostructured AAO films with pore size of 40–300 nm and thickness of 50–250 μm is common [22–27]. For example, Dotzauer et al. [25], immobilized gold nanoparticles on nanopore supports of AAO with a pore size of 200 nm and a thickness of 20 μm, for the reduction of 4-nitrophenol. Ganley et al. [26] manufactured aluminum-alumina catalytic microreactors for the decomposition of ammonia into hydrogen and nitrogen, with thickness between 50 and 60 μm. Milka et al. [27] successfully immobilized Alliinase in AAO membrane filters of 200 nm pore diameter. On the other hand, in applications of filtration and molecular separation, AAO membranes with pore size of 10–185 nm, interpore distance of 50–140 nm and film thickness of 0.7–1 μm were used [28–30].

Based on the fact that it is fundamental to select the synthesis conditions that best adapt to each particular application, we also studied the correlation between the synthesis conditions (electrolyte concentration, temperature and anodization voltage), the current density vs. time curves [3,4,11,31] and the morphological properties of the AAO films, defined mainly by the pore diameter, the interpore distance, pore density and the film thickness.

2. Materials and Methods

2.1. Substrate Material

The substrate used was a sheet of the commercial aluminum alloy AA 1050 (supplied by AMEX® S.A., Buenos Aires, Argentina), whose composition in is detailed Table 1. In addition, Figure A1 (Appendix A) shows mappings of the main elements of AA 1050 (Al, Fe and Si) carried out by X-ray energy dispersion spectrometry.

Specimens of approximately 1 cm wide, 3 cm high and 0.3 cm thick were cut. The specimens were included in commercial acrylic (Subiton, San Fernando, Argentina) to isolate the edges and one of the faces, delimiting the exposed area of the specimens to 3 cm^2.

Table 1. Chemical composition of commercial AA 1050 (weight percent) [32].

Element	Al	Fe	Si	Cu	Zn	Ti	V	Mg	Mn
Min.	99.50	0.12	0.07	–	–	–	–	–	–
Max.	–	0.30	0.20	0.051	0.05	0.03	0.05	0.05	0.05

2.2. Synthesis of AAO Coatings

2.2.1. Pre-Treatment of the Substrate Surface

Prior to anodization [33], the surface of the substrate was prepared in the following stages: (i) grinding in a rotary plate polisher (Struers, Ballerup, Denmark) at 250 rpm, with SiC sandpaper of decreasing granulometry from # 280 to # 2500 (Doble A and Norton); (ii) polishing in a rotary

plate polisher (Struers, Ballerup, Denmark) at 250 rpm with diamond pastes of 6 (Prazis, Buenos Aires, Argentina) and 1 μm (Prazis, Buenos Aires, Argentina) for 1 h each on a cloth (Prazis, Buenos Aires, Argentina) by using ethylene glycol (Biopack, Buenos Aires, Argentina) as lubricant; (iii) electropolishing in a 3.5:4:2.5 *V*/*V* ethanol 96% (Biopack, Buenos Aires, Argentina): 85% phosphoric acid (Anedra, Buenos Aires, Argentina): water solution, vigorously stirring the solution at 40 °C with a magnetic stirrer with heating control (78HW-1, Arcano, Nanjing, China), at 60 V with limitation of current density in 0.25 A/cm^2 for 3 min, using two sources (TPR3003T, Atten, Shenzhen, China) connected in series in potentiostatic mode and cathode of aluminum 99.999% (supplied by Aluar, Buenos Aires, Argentina) of 6 cm^2 of submerged area; and iv) attack in solution of 6% by weight of 85% phosphoric acid (Anedra, Buenos Aires, Argentina), 1.8% by weight of chromic acid (Cicarelli, Santa Fe, Argentina), 92.2% by weight of distilled water at 60 °C for 3 h. At the end of each pre-treatment stage, the specimens were cleaned with distilled water to remove any unwanted residue from the previous stage, sprayed with alcohol and dried with hot air.

2.2.2. Anodic Oxidation

Coatings were synthesized by means of a single 1-h anodization step, circulating direct current, using two sources (TPR3003T, Atten, Shenzhen, China) connected in series in potentiostatic mode and with magnetic stirring with heating control (78HW-1, Arcano, Nanjing, China) of the electrolyte. A platinum plate (99.999%, Roberto Cordes S.A., Buenos Aires, Argentina) of 12 cm^2 of exposed area was used as cathode to oxidize 1 cm^2 of pre-treated AA 1050 (anode). The parameters that were varied in each synthesis were: Electrolyte concentration (*C*) (0.3 and 0.9 M), electrolyte temperature (*T*) (20, 30 and 40 ± 2 °C) and anodization voltage (*V*) (30, 40 and 60 V). The selection of the experimental conditions was made based on the ranges of temperature, concentration of oxalic acid and voltage presented by Sulka [3], with the aim of widening the AAO films synthesis conditions and characterization, until now not thoroughly studied.

During the anodization process, the current density (j) was recorded as a function of the anodization time. All tests were performed in duplicate. The specimens were named with the letter O and a number indicating the concentration (in Molar) of the oxalic acid used, followed by the letter T and a number corresponding to the temperature (in °C) of the electrolyte, and finally the letter V and the voltage (in Volts) used in the anodization process. For example, the test piece O0.3 T20 V30 corresponded to a test piece anodized with 0.3 M oxalic acid at 20 °C and 30 V.

2.3. Morphological Characterization of Coatings

The nanopores in the anodic films were characterized by scanning electron microscopy (SEM), using a SUPRA 40 (Carl Zeiss NTS GmbH, Buenos Aires, Argentina) equipment. The average pore diameter ($\overline{dp}$), the interpore distance ($\overline{di}$) and the pore density ($\overline{\rho}$) were determined from SEM micrographs with the free software ImageJ (1.50i version) [34–36], as follows: $\overline{dp}$ was calculated from the area of the pores identified in a SEM image magnified 80000 times, using the particle analysis tool; $\overline{di}$, was estimated from 20 measurements made from the center of one pore to the center of another; and $\overline{\rho}$ was determined by counting the number of pores per unit area.

The average thickness ($\overline{e}$) of the oxide films was determined by observing the cross-section of the sample under an optical microscope (EPIPHOT, Nikon, Japan), making 10 measurements for each case. Previously, the cross sections of the samples have grinded to facilitate the identification of the oxide film from the substrate in the microscope.

3. Results and Discussion

3.1. Influence of Variables (C, T and V) During the Synthesis of AAO Films—Current Density vs. Time Curves

Figure 1 shows the variation of the current density (*j*) as a function of the time recorded during anodization in 0.3 M (Figure 1a) and 0.9 M oxalic acid (Figure 1b) at 20, 30 and 40 °C and 30, 40 and 60 V. From the analysis of the curves, current density vs. time of Figure 1a,b, we summarized in Figure 1c the anodic pore formation in four characteristic curves related to the conditions of anodic synthesis. The curve (1) of Figure 1c stands for the behavior of anodization of O0.3 T20 V(30–40) and O0.9 T20 V30; the curve (2) stands for the behavior of anodization of O0.3 T20 V60; the curve (3) corresponds to the anodizations of O0.3 T(30–40) V(30–40), O0.9 T20 V40 and O0.9 T(30–40) V(30–40); and the curve (4) corresponds to the anodizations of O0.3 T(30–40) V60.

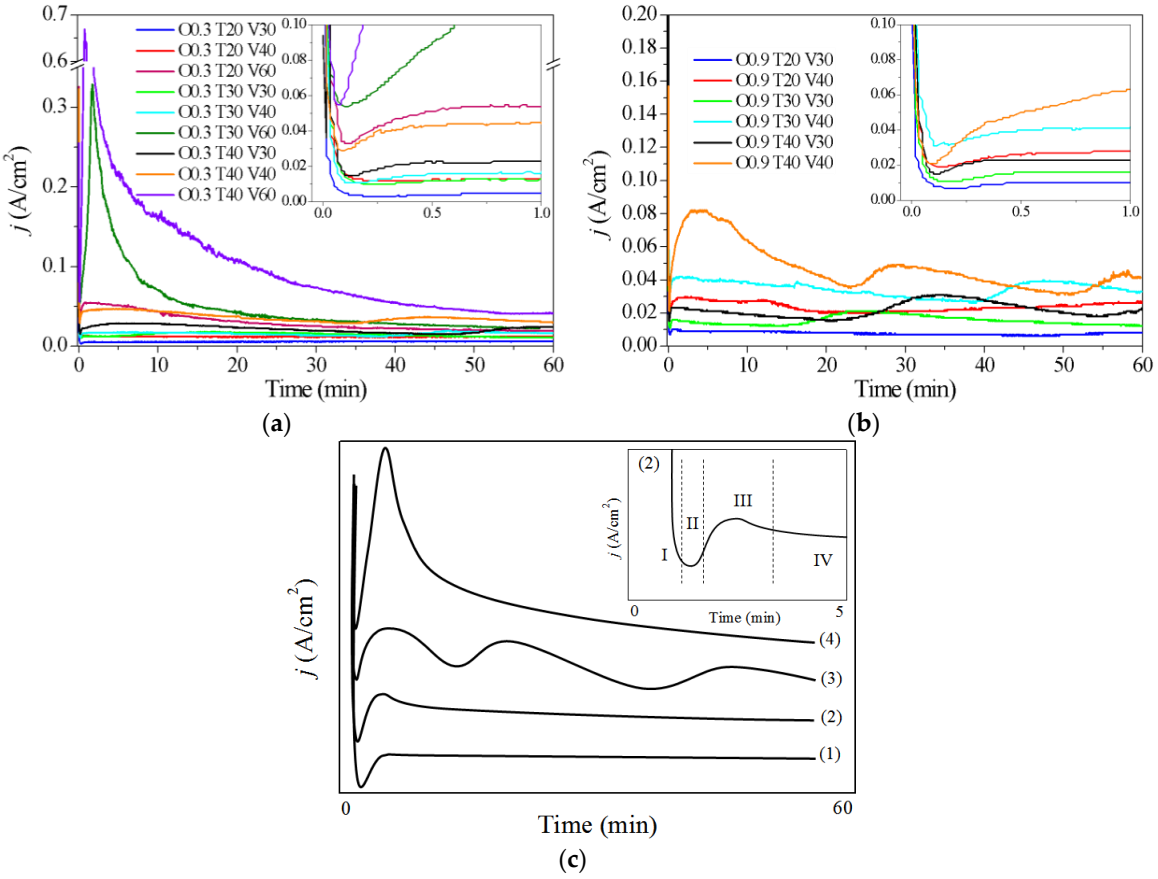

Figure 1. Current density (*j*) vs time recorded during the first anodization step in 0.3 M (**a**) and 0.9 M (**b**) oxalic acid at different voltages and temperatures; insets: first stages of anodization. Current density vs. time curves representative of anodic behavior in different synthesis conditions (**c**); inset: stages of pore growth: I: formation of barrier layer, II: formation of pore precursor pits, III: formation of pores and IV: growth in of pores stationary state (Inset adapted from Sulka [3]).

In general, curves (1) and (2) show four stages corresponding to the process of formation of porous AAO films (Figure 1c). During stage I, there is an abrupt decrease in the current density at the beginning of the anodization process until a minimum value is reached, due to the growth of a compact and uniform oxide layer of the barrier type, which progressively increases the resistance of the system to the passage of current [2,3]. In stage II, the process of nucleation of the pores and the initial growth of the porous structure is initiated by dissolution of the barrier oxide layer assisted by the electric field. Then, in stage III, current density increases over time to a maximum, due to the rupture of the barrier

layer and the rapid diffusion of the electrolyte through the oxide. The presence of a maximum in the curve indicates the rearrangement of the porous structure [3]. Finally, in stage IV, the pores reach a stationary growth and the barrier type layer is dissolved. This stage is characterized by a slow decrease in the current density until reaching an equilibrium value [3,4,19,37]. Particularly, curves (3) and (4) do not seem to reach stage IV during the anodizing time of 1 h. This could be due to much more reactive oxidation and dissolution reactions of the oxide layer that occurs at high concentrations of oxalic acid, high electrolyte temperatures and high anodization voltages. The curve (3) shows several undulations that imply little stability in the process of anodic film growth, possibly attributed to the dissolution of preferential sites of the porous layer (e.g., the surface inhomogeneities, the residual stresses of the material and the presence of impurities) and its subsequent oxidation. On the other hand, curve (4) shows pronounced peaks of current density in stage III, which could be attributed to higher dissolution rates than oxide growth rates [38], which may allow several adjacent pores to merge to generate larger pores [4]. The latter is characteristic for anodization at 60 V and high temperatures, where the maximum of j reached in stage III exceeds 0.3 A/cm^2 (Figure 1a) and correlate with the morphologies described in Section 3.2 below.

Comparatively, the current density vs. time curves in Figure 1a,b show an increase in the current density values at all stages of the anodization process with the increase in temperature and voltage. It can be observed in the insets of Figure 1a,b that the minimum current density corresponding to stage I of pore growth occurs faster and that higher current values are reached with increasing voltage and temperature of the solution, in accordance with that previously reported by Sulka [3].

The effect of oxalic acid concentration on anodic synthesis can be observed by comparing the initial current density peaks for each synthesis condition. In general, an increase in the initial maximum j is observed with the increase in acid concentration, a fact that favors mainly the dissolution process (stage III). Such is the case that, during anodic oxidations in 0.9 M oxalic acid at 60 V at different temperatures, an excessive dissolution of the oxide was induced, causing an increase in the current density (up to around 2 A/cm^2) and an uncontrollable increase in the temperature of the solution (results not shown), which made anodic synthesis impossible for 1 h under such conditions.

3.2. Influence of Variables (C, T and V) on the Morphology of Coatings

Figures 2 and 3 show the SEM micrographs of the AAO coatings obtained at different temperatures and voltages and with 0.3 and 0.9 M oxalic acid, respectively. In all cases, nanoporous structures, with three types of structures, can be observed: (A) defined by branched pores (pores within pores), predominant in synthesis at 30 V and 20 and 30 °C; (B) defined by unbranched pores of thin wall, as a consequence of high synthesis temperatures and voltages; (C) defined as the transition from the first structure to the second, because voltage and temperature increases with respect to the minimum levels evaluated (20 °C and 30 V). These morphological differences observed in the porous structure of the AAO films coincide with the results described in the analysis of the current density vs. time curves for each synthesis condition. Thus, the formation of branched pores may be due to low rates of oxide dissolution and lack of reordering of the porous matrix, while the non-branching of pores may be achieved with higher rates of oxidation and dissolution, as the voltage and temperature of synthesis increase.

Figure 4 shows the variation of the morphological parameters of nanostructured AAO films synthesized in 0.3 and 0.9 M oxalic acid as a function of voltage and temperature, and Table 2 shows the mean values and dispersion of these parameters for each structure. Figure 4a shows the variation of the average pore diameter ($\overline{dp}$) with the anodizing voltage [3,9] and the electrolyte temperature [3,39]. In the films synthesized in 0.3 M oxalic acid, at 20 °C, although the error bars of $\overline{dp}$ overlapped and the differences were not significant between 30 and 40 V and between 40 and 60 V, the increase in $\overline{dp}$ with the voltage was clear and significant between 30 and 60 V, with pore sizes ranging between 21 and 38 nm. The same occurs with AAO films synthesized at a constant temperature of 30 °C, with $\overline{dp}$ ranging between 29 and 80 nm with 30 and 60 V, respectively. However, at 40 °C the increase of $\overline{dp}$, is significant in the whole range of voltage studied, 30, 40 and 60 V, with mean values of 35.9, 64.0

and 97.4 nm, respectively. This could be due to an increase in oxide dissolution assisted by an electric field and favored by increased oxide solubility at high temperatures [3]. Moreover, for each constant anodizing voltage, the $\overline{dp}$ increase with temperature between 20 and 40 °C, and the range of increase is higher with higher voltage.

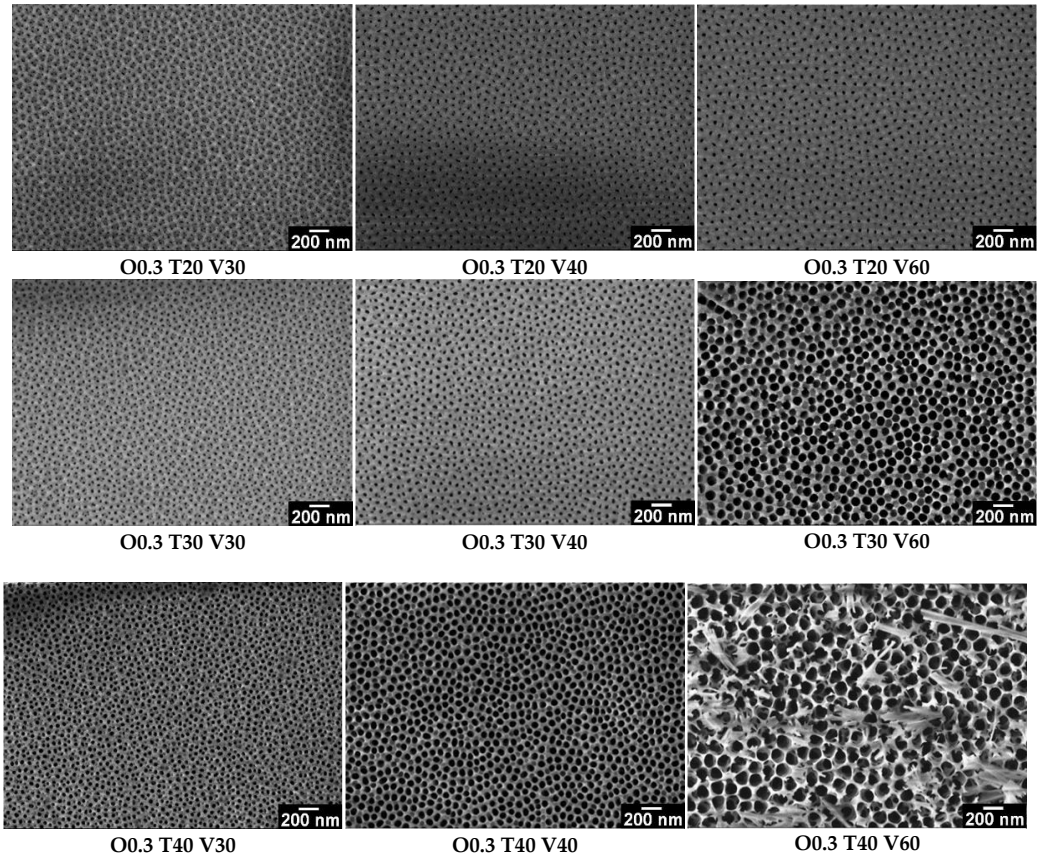

Figure 2. SEM images of nanostructured anodic aluminum oxide (AAO) films obtained by means of a one-step anodization process of 1 h in 0.3 M oxalic acid at different temperatures and voltages.

Table 2. Average values of the morphological parameters of nanostructured AAO coatings obtained in 0.3 and 0.9 M oxalic acid at different temperatures and anodization voltages (*C* is the oxalic acid concentration, *T* the electrolyte temperature, *V* the anodization voltage and *S* is the nanoporous structure).

Sample	*C* (M)	*T* (°C)	*V* (V)	*S*	$\overline{dp}$ (nm)	$\overline{di}$ (nm)	$\overline{\rho}$ (pores/cm^2)	$\overline{e}$ (μm)
O0.3 T20 V30	0.3	20	30	A	20.8 ± 5.6	58.9 ± 6.0	$2.7 \times 10^{10} \pm 2.0 \times 10^{9}$	14.6 ± 1.2
O0.3 T20 V40	0.3	20	40	B	35.2 ± 8.2	90.9 ± 12.8	$1.7 \times 10^{10} \pm 8.4 \times 10^{8}$	18.7 ± 1.6
O0.3 T20 V60	0.3	20	60	B	37.5 ± 3.1	116.0 ± 14.5	$1.0 \times 10^{10} \pm 8.9 \times 10^{8}$	80.3 ± 0.8
O0.3 T30 V30	0.3	30	30	A	28.5 ± 7.3	59.2 ± 11.8	$2.6 \times 10^{10} \pm 7.1 \times 10^{8}$	21.3 ± 0.9
O0.3 T30 V40	0.3	30	40	B	34.1 ± 6.4	88.2 ± 9.2	$1.5 \times 10^{10} \pm 1.6 \times 10^{8}$	30.3 ± 2.8
O0.3 T30 V60	0.3	30	60	C	80.5 ± 7.3	115.1 ± 19.7	$8.6 \times 10^{9} \pm 2.5 \times 10^{8}$	144.6 ± 7.5
O0.3 T40 V30	0.3	40	30	A	35.9 ± 7.9	73.6 ± 10.0	$2.6 \times 10^{10} \pm 1.0 \times 10^{9}$	28.4 ± 0.8
O0.3 T40 V40	0.3	40	40	C	64.0 ± 4.2	91.3 ± 7.5	$1.3 \times 10^{10} \pm 4.3 \times 10^{8}$	75.5 ± 1.0
O0.3 T40 V60	0.3	40	60	C	97.4 ± 27.6	138 ± 20.1	$5.4 \times 10^{9} \pm 7.2 \times 10^{8}$	124.2 ± 2.8
O0.9 T20 V30	0.9	20	30	A	24.1 ± 5.7	63.4 ± 13.8	$3.0 \times 10^{10} \pm 1.5 \times 10^{9}$	19.7 ± 0.6
O0.9 T20 V40	0.9	20	40	A	21.1 ± 6.1	62.7 ± 17.8	$2.8 \times 10^{10} \pm 2.3 \times 10^{8}$	38.2 ± 1.0
O0.9 T30 V30	0.9	30	30	A	23.4 ± 6.3	61.7 ± 11.9	$2.6 \times 10^{10} \pm 2.0 \times 10^{8}$	34.4 ± 1.4
O0.9 T30 V40	0.9	30	40	B	26.9 ± 5.0	61.5 ± 10.7	$2.6 \times 10^{10} \pm 4.8 \times 10^{8}$	77.8 ± 0.7
O0.9 T40 V30	0.9	40	30	C	44.6 ± 6.4	62.8 ± 7.5	$1.9 \times 10^{10} \pm 9.1 \times 10^{8}$	66.0 ± 2.0
O0.9 T40 V40	0.9	40	40	C	63.8 ± 7.8	88.3 ± 9.3	$1.4 \times 10^{10} \pm 6.8 \times 10^{8}$	80.2 ± 3.0

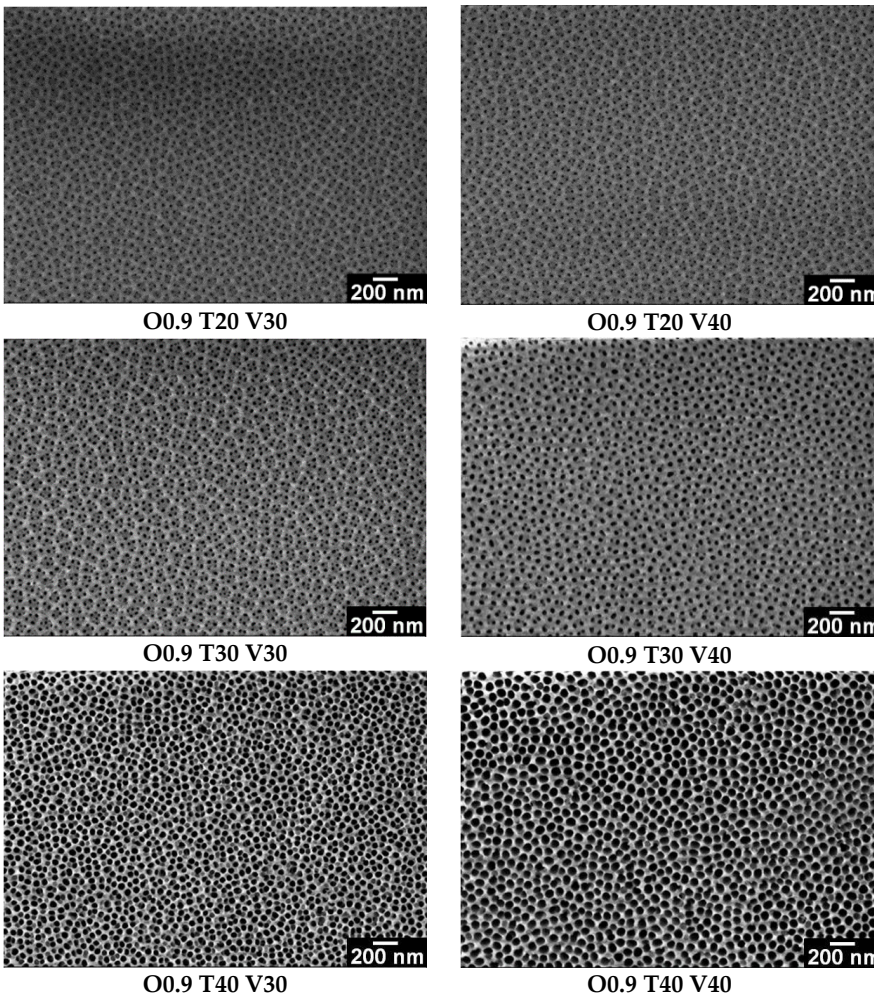

Figure 3. SEM images of nanostructured AAO films by means of a one-step anodization process of 1 h in 0.9 M oxalic acid at different temperatures and voltages.

For films synthesized in 0.9 M oxalic acid, there were no variation of $\overline{dp}$ with increases in voltage (from 30 to 40 V) and electrolyte temperature of 20 and 30 °C ($\overline{dp} \cong 24$ nm), but $\overline{dp}$ increased with voltage at 40 °C, from 45 (30 V) to 64 nm (40 V) (Figure 4a). Thus, it can be seen that, for both oxalic acid concentrations, the highest $\overline{dp}$ values were obtained with the highest temperature and voltage levels. On the other hand, the increase in oxalic acid concentration from 0.3 to 0.9 M had a negligible effect on the $\overline{dp}$ at 30 and 40 V (Figure 4a).

Figure 4b shows that the average interpore distance ($\overline{di}$) increased from 59 to 138 nm with the increases in voltage and temperature in oxalic acid 0.3 M. However, $\overline{di}$ values did not show significant differences at 20, 30 and 40 °C. For films synthesized in 0.9 M oxalic acid, the variation of $\overline{di}$ with the increase in voltage (from 30 to 40 V) was observed only at 40 °C, with $\overline{di}$ values of 63 to 88 nm, whereas, at 20 and 30 °C, $\overline{di}$ remained constant at 62 nm. In this sense, it was also observed that the combination of high voltages and temperatures gave rise to the highest values of $\overline{di}$ and vice versa. In addition, the effect of the concentration of oxalic acid on $\overline{di}$ was negligible at 30 and 40 V. It should be noted that the $\overline{di}$ in type A and B structures was measured by calculating the distances between primary and secondary pores. This explains the greater dispersion obtained in the estimation of the values of $\overline{di}$, which can be observed in the error bars of Figure 4b.

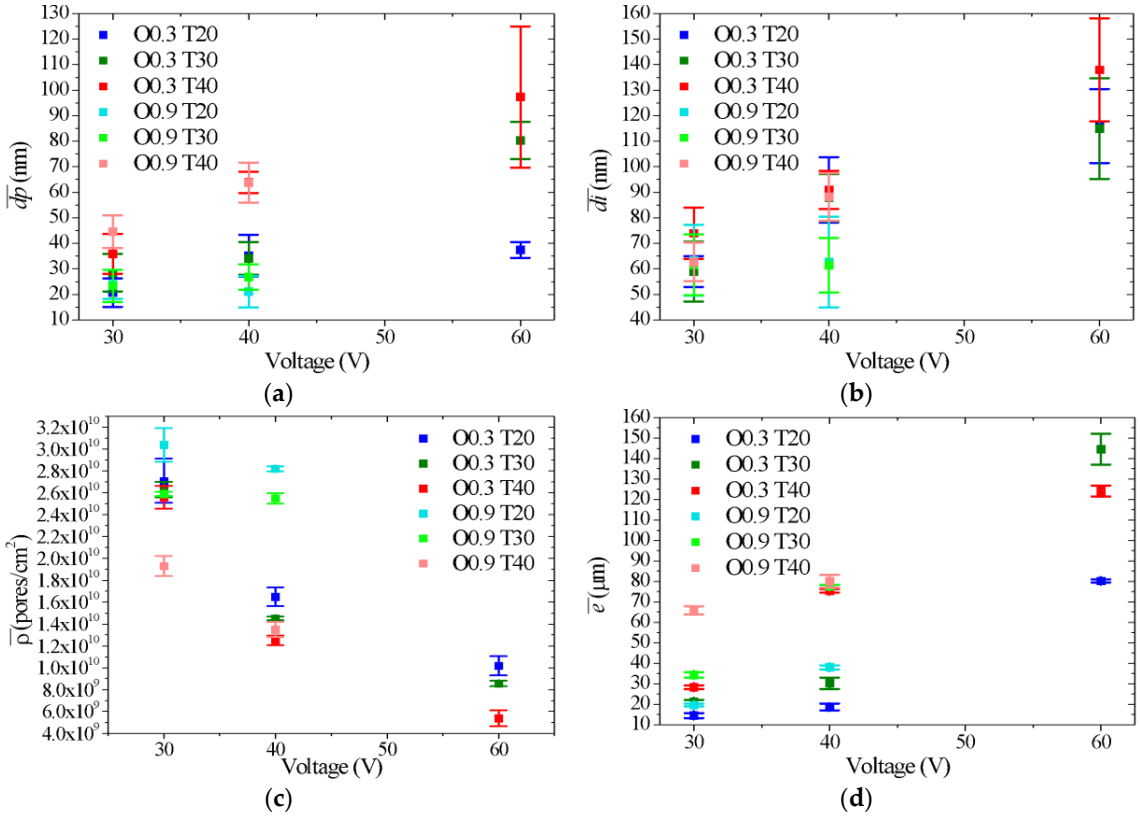

Figure 4. Variation of average pore diameter (**a**), average interpore distance (**b**), average pore density (**c**) and average thickness (**d**) of nanostructured AAO films synthesized by means of a one-step anodization process in 0.3 and 0.9 M oxalic acid as a function of voltage and temperature.

Figure 4c shows the variation of pore density ($\overline{\rho}$) of the nanostructured AAO coatings synthesized in 0.3 and 0.9 M oxalic acid as a function of temperature and voltage. For coatings obtained in 0.3 M oxalic acid, the highest $\overline{\rho}$ (2.7×10^{10} pores/cm^2) was obtained at 20 °C and 30 V, while the lowest (5.4×10^{9} pores/cm^2) was obtained at 40 °C and 60 V. Likewise, for coatings obtained in 0.9 M acid, the maximum $\overline{\rho}$ was observed at 20 °C and 30 V, while, as the voltage and temperature of the electrolyte increased, $\overline{\rho}$ decreased. This decrease was consistent with the increase in $\overline{dp}$ and $\overline{di}$ observed at high voltages and temperatures. On the other hand, significant differences were observed in $\overline{\rho}$ when increasing the oxalic acid concentration from 0.3 to 0.9 M at 40 V and 20–30 °C, with an increase of approximately 1.2×10^{10} pores/cm^2. Likewise, the decrease in $\overline{\rho}$ at 30 V and 40 °C, with respect to the values measured for the other synthesis temperatures, was notable. This could indicates that the process of nanopore formation is a complex mechanism that strongly depends on the combination of anodic synthesis variables.

Figure 4d shows the thicknesses ($\overline{e}$) of the coatings synthesized in 0.3 and 0.9 M oxalic acid as a function of the anodizing temperature and voltage. In Figure A2 (Appendix A) optical micrographs of the thickness of some samples synthesized in different anodization conditions are presented. In general, an increase in $\overline{e}$ can be seen with increases in oxalic acid concentration, electrolyte temperature and voltage. Thus, at 30 V in 0.3 M oxalic acid, $\overline{e}$ increased by 15, 21 and 28 μm as temperature increased to 20, 30 and 40 °C respectively, whereas at a constant temperature of 30 °C, $\overline{e}$ increased by 21, 30 and 145 μm as voltage increased to 30, 40 and 60 V, respectively. In addition, the increase in oxalic concentration from 0.3 to 0.9 M for each combination of temperature and voltage allowed thickness to increase from 4 to 48 μm.

The longitudinal growth of the pores depends on the dynamic equilibrium between oxidation and oxide dissolution [9]. In this sense, high values of acid concentration, electrolyte temperature and voltage increase the rates of oxidation and dissolution of the barrier layer, and consequently increase

the thickness of the coating. Particularly, the increase of the electrolyte concentration generates a greater ionic conductivity that increases the rate of oxide growth, producing thicker coatings [9]. This can be correlated with the current density vs. time curves in Figure 1a,b by comparing the current density values recorded in each of the anodization stages. However, certain conditions of anodic synthesis, such as O0.3 T40 V60 and O0.9 T40 V40, favored the oxide dissolution process over the oxidation process, limiting the growth of the porous layer to high voltages and electrolyte temperatures.

Depending on the anodization conditions used, the nanoporous AAO coatings obtained showed $\overline{dp}$ values between 21 and 97 nm, $\overline{di}$ between 59 and 138 nm, $\overline{\rho}$ between 2.8×10^{10} and 5.4×10^{9} pores/cm^2 and $\overline{e}$ between 15 and 145 μm. Although the morphology of the nanopores obtained is far from the ideal hexagonal packaging defined by a central pore surrounded by six neighboring pores, typical of AAO films obtained by a two-step anodization process [35], this characteristic is not a limiting factor to promote technological applications such as catalysis, filtration and molecular separation. In addition, since these nanopores were obtained by means of a one-step anodization process, the costs and time synthesis are considerably reduced.

4. Conclusions

In this study, aluminum oxide coatings were synthesized with a low-cost, single-step anodization process under various experimental conditions, and pore diameter, interpore distance, pore density and film thickness were measured. The results obtained allow concluding that:

- By varying the oxalic acid concentration (0.3 and 0.9 M), the electrolyte temperature (20, 30 and 40 °C) and the voltage (30, 40 and 60 V), it is possible to obtain nanoporous AAO coatings with $\overline{dp}$ values between 21 and 97 nm, $\overline{di}$ between 59 and 138 nm, $\overline{\rho}$ between 2.8×10^{10} and 5.4×10^{9} pores/cm^2 and $\overline{e}$ between 15 and 145 μm. In this way, selecting the appropriate combination of synthesis variables allows synthesizing AAO coatings with the morphological characteristics that best suit each particular application, mainly in catalysis, where pore sizes between 40 and 300 nm and thicknesses between 50–250 μm are commonly required.
- The pore diameter, interpore distance and pore density of anodic films vary significantly with the voltage and temperature of the electrolyte. In general, the highest values of $\overline{dp}$ and $\overline{di}$ were obtained with the highest levels of voltage and temperature, whereas the highest values of $\overline{\rho}$ were obtained with the lowest levels of voltage, temperature and concentration.
- Film thickness increased with increases in oxalic acid concentration, electrolyte temperature and voltage. However, certain anodic synthesis conditions favored the oxide dissolution process over the oxidation process, limiting the growth in thickness.
- The shape of the anodic curves strongly depended on the concentration of oxalic acid, temperature and anodizing voltage. These results coincide with those obtained from the characterization by optical microscopy and scanning microscopy, demonstrating the usefulness of the current density vs. time curves to predict some morphological characteristics of the oxides in a simple and fast way.

Author Contributions: Conceptualization, F.A.B. and G.R.K.; Methodology, F.A.B. and G.R.K.; Software, F.A.B.; Formal Analysis, F.A.B., G.R.K. and M.L.V.; Investigation, F.A.B. and M.L.V.; Resources, A.E.A.; Writing—Original Draft Preparation, F.A.B. and G.R.K.; Writing—Review and Editing, M.L.V. and A.E.A.; Supervision, M.L.V. and A.E.A.; Project Administration, A.E.A.; Funding Acquisition, A.E.A.

Funding: This research was funded by Consejo Nacional de Investigaciones Científicas y Técnicas (CONICET) and Agencia Nacional de Promoción Científica y Tecnológica (ANPCyT) of Argentina (PICT-2017-0079), and also funded by the scholarship from CONICET.

Conflicts of Interest: The authors declare no conflict of interest.

Appendix A

X-ray energy dispersion spectrometry (EDS) mapping of substrate AA 1050 was performed in SUPRA 40 scanning electronic microscope (Carl Zeiss NTS GmbH, Buenos Aires, Argentina, Figure A1).

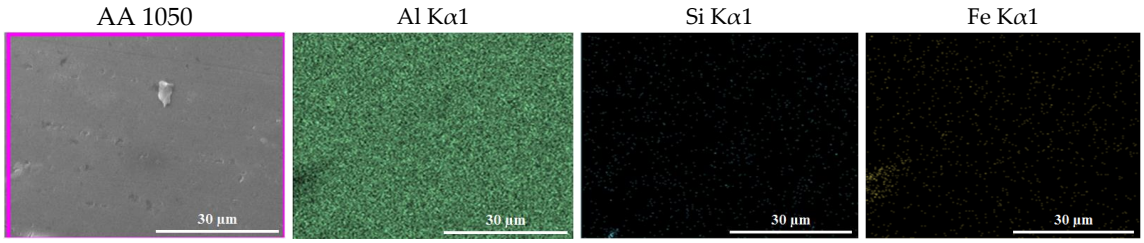

Figure A1. EDS mapping of AA 1050.

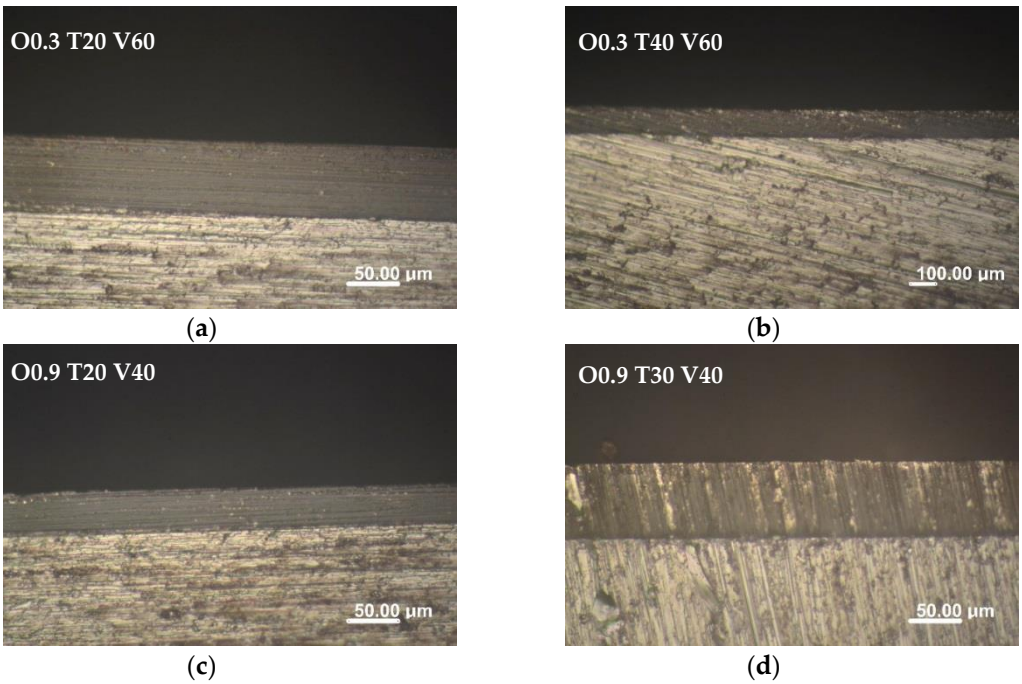

Figure A2. Optical micrograph of the cross-section of AAO film obtained by means of a one-step anodization process of 1 h in 0.3 and 0.9 M oxalic acid at different temperatures and voltages.

References

1. Bai, A.; Hu, C.-C.; Yang, Y.-F.; Lin, C.-C. Pore diameter control of anodic aluminum oxide with ordered array of nanopores. *Electrochimica Acta* **2008**, *53*, 2258–2264. [CrossRef]
2. Cheng, C. *Electro-Chemo-Mechanics of Anodic Porous Alumina Nano-Honeycombs: Self-Ordered Growth and Actuation*; Springer: Berlin/Heidelberg, Germany, 2015; pp. 1–166.
3. Sulka, G.D. Highly ordered anodic porous alumina formation by self-organized anodizing. In *Nanostructured Materials in Electrochemistry*; WILEY-VCH: Weinheim, Germany, 2008; Volume 1, pp. 1–116.
4. Jani, A.M.M.; Losic, D.; Voelcker, N.H.; Jani, A.M. Nanoporous anodic aluminium oxide: Advances in surface engineering and emerging applications. *Prog. Mater. Sci.* **2013**, *58*, 636–704. [CrossRef]
5. Masuda, H.; Fukuda, K. Ordered metal nanohole arrays made by a two-step replication of honeycomb structures of anodic alumina. *Science* **1995**, *268*, 1466–1468. [CrossRef] [PubMed]
6. Vrublevsky, I.; Parkoun, V.; Sokol, V.; Schreckenbach, J.; Marx, G. The study of the volume expansion of aluminum during porous oxide formation at galvanostatic regime. *Appl. Surf. Sci.* **2004**, *222*, 215–225. [CrossRef]

7. Nielsch, K.; Choi, J.; Schwirn, K.; Wehrspohn, R.B.; Gösele, U. Self-ordering regimes of porous alumina: The 10% porosity rule. *Nano Lett.* **2002**, *2*, 677–680. [CrossRef]
8. Li, A.P.; Müller, F.; Birner, A.; Nielsch, K.; Gösele, U. Hexagonal pore arrays with a 50–420 nm interpore distance formed by self-organization in anodic alumina. *J. Appl. Phys.* **1998**, *84*, 6023–6026. [CrossRef]
9. Belwalkar, A.; Grasing, E.; Van Geertruyden, W.; Huang, Z.; Misiolek, W.Z. Effect of processing parameters on pore structure and thickness of anodic aluminum oxide (AAO) tubular membranes. *J. Membr. Sci.* **2008**, *319*, 192–198. [CrossRef] [PubMed]
10. Ghorbani, M.; Nasirpouri, F.; Saedi, A. On the growth sequence of highly ordered nanoporous anodic aluminium oxide. *Mater. Des.* **2006**, *27*, 983–988. [CrossRef]
11. Han, X.Y.; Shen, W.Z. Improved two-step anodization technique for ordered porous anodic aluminum membranes. *J. Electroanal. Chem.* **2011**, *655*, 56–64. [CrossRef]
12. Zhang, F.; Liu, X.; Pan, C.; Zhu, J. Nano-porous anodic aluminum oxide membranes with 6–19 nm pore diameters formed by a low-potential anodizing process. *Nanotechnology* **2007**, *18*, 345302. [CrossRef]
13. Chung, C.K.; Liao, M.W.; Chang, H.C.; Lee, C.T. Effects of temperature and voltage mode on nanoporous anodic aluminum oxide films by one-step anodization. *Thin Solid Films* **2011**, *520*, 1554–1558. [CrossRef]
14. Stępniowski, W.J.; Bojar, Z. Synthesis of anodic aluminum oxide (AAO) at relatively high temperatures. Study of the influence of anodization conditions on the alumina structural features. *Surf. Coat. Technol.* **2011**, *206*, 265–272. [CrossRef]
15. Jessensky, O.; Müller, F.; Gösele, U. Self-organized formation of hexagonal pore arrays in anodic alumina. *Appl. Phys. Lett.* **1998**, *72*, 1173–1175. [CrossRef]
16. Na, H.C.; Sung, T.J.; Yoon, S.H.; Hyun, S.K.; Kim, M.S.; Lee, Y.G.; Shin, S.H.; Choi, S.M.; Yi, S. Formation of unidirectional nanoporous structures in thickly anodized aluminum oxide layer. *Trans. Nonferrous Met. Soc. China* **2009**, *19*, 1013–1017. [CrossRef]
17. Pardo-Saavedra, D.C; Londoño-Calderón, C.L.; Menchaca-Nal, S.; Pampillo, L.G.; Martínez García, R.; Socolovsky, L.M. Morfological study of pore widening process in anodized alumina films. *An. AFA* **2013**, *25*, 68–71. [CrossRef]
18. Zaraska, L.; Sulka, G.D.; Szeremeta, J.; Jaskuła, M. Porous anodic alumina formed by anodization of aluminum alloy (AA1050) and high purity aluminum. *Electrochim. Acta* **2010**, *55*, 4377–4386. [CrossRef]
19. Londoño Calderón, C.L.; Menchaca Nal, S.; Pardo Saavedra, D.C.; Silveyra, J.M.; Socolovsky, L.M.; Pampillo, L.G.; Martínez García, R. Low cost fabrication of porous anodic alumina: A comparative study of the morphology produced by one- and two-steps of anodization. *RevistMatéria* **2016**, *21*, 677–690.
20. Nasirpouri, F.; Abdollahzadeh, M.; Almasi, M.J.; Parvini-Ahmadi, N. A comparison between self-ordering of nanopores in aluminium oxide films achieved by two- and three-step anodic oxidation. *Curr. Appl. Phys.* **2009**, *9*, S91–S94. [CrossRef]
21. Hurtado, M.J.; Capitán, M.J.; Alvarez, J.; Fatás, E.; Herrasti, P. The anodic oxidation of aluminum: Fabrication and characterization. *Portugaliae Electrochim. Acta* **2007**, *25*, 153–162. [CrossRef]
22. Ingham, C.J.; ter Maat, J.; de Vos, W.M. Where bio meets nano: The many uses for nanoporous aluminum oxide in biotechnology. *Biotechol. Adv.* **2012**, *30*, 1089–1099. [CrossRef]
23. Poinern, G.E.J.; Ali, N.; Fawcett, D. Progress in nano-engineered anodic aluminum oxide membrane development. *Materials* **2011**, *4*, 487–526. [CrossRef]
24. Stair, P.C.; Marshall, C.; Xiong, G.; Feng, H.; Pellin, M.J.; Elam, J.W.; Curtiss, L.; Iton, L.; Kung, H.; Kung, M.; et al. Novel, uniform nanostructured catalytic membranes. *Top. Catal.* **2006**, *39*, 181–186. [CrossRef]
25. Dotzauer, D.M.; Dai, J.; Sun, L.; Bruening, M.L. Catalytic membranes prepared using layer-by-layer adsorption of polyelectrolyte/metal nanoparticle films in porous supports. *Nano Lett.* **2006**, *6*, 2268–2272. [CrossRef] [PubMed]
26. Ganley, J.C.; Riechmann, K.L.; Seebauer, E.G.; Masel, R.I. Porous anodic alumina optimized as a catalyst support for microreactors. *J. Catal.* **2004**, *227*, 26–32. [CrossRef]
27. Milka, P.; Krest, I.; Keusgen, M. Immobilization of alliinase on porous aluminum oxide. *Biotechnol. Bioeng.* **2000**, *69*, 344–348. [CrossRef]
28. Itaya, K.; Sugawara, S.; Arai, K.; Saito, S. Properties of porous anodic aluminum oxide films as membranes. *J. Chem. Eng. Jpn.* **1984**, *17*, 514–520. [CrossRef]
29. Thormann, A.; Teuscher, N.; Pfannmçller, M.; Rothe, U.; Heilmann, A. Nanoporous aluminum oxide membranes for filtration and biofunctionalization. *Small* **2007**, *3*, 1032–1040. [CrossRef]

30. Osmanbeyoglu, H.U.; Hur, T.B.; Kim, H.K. Thin alumina nanoporous membranes for similar size biomolecule separation. *J. Membr. Sci.* **2009**, *343*, 1–6. [CrossRef]
31. Sulka, G.D.; Stepniowski, W.J. Structural features of self-organized nanopore arrays formed by anodization of aluminum in oxalic acid at relatively high temperatures. *Electrochim. Acta* **2009**, *54*, 3683–3691. [CrossRef]
32. Hodgson, D.E.; Wu, M.H.; Biermann, R.J. *ASM Handbook, Volume 2, Properties and Selection: Nonferrous Alloys and Special-Purpose Materials*; ASM International: Novelty, OH, USA, 1990; pp. 1–1328.
33. Bruera, F.A.; Kramer, G.R.; Vera, M.L.; Ares, A.E. Selección de pretratamientos superficiales para la síntesis de recubrimientos anódicos nanoestructurados de Al 1050. In *6° Encuentro de Jóvenes Investigadores en Ciencia y Tecnología de Materiales—JIM 2017, Buenos Aires, Argentina, 17–18 August 2017*; Argentinian Association of Crystallography: Buenos Aires, Argentina, 2017; pp. 547–550. (In Spanish)
34. Schneider, C.A.; Rasband, W.S.; Eliceiri, K.W. NIH Image to ImageJ: 25 years of image analysis. *Nat. Methods* **2012**, *9*, 671–675. [CrossRef]
35. Vojkuvka, L.; Marsal, L.F.; Ferré-Borrull, J.; Formentin, P.; Pallarés, J. Self-ordered porous alumina membranes with large lattice constant fabricated by hard anodization. *Superlattices Microstruct.* **2008**, *44*, 577–582. [CrossRef]
36. Sulka, G.D.; Parkola, K.G. Anodising potential influence on well-ordered nanostructures formed by anodisation of aluminium in sulphuric acid. *Thin Solid Films* **2006**, *515*, 338–345. [CrossRef]
37. Lee, W.; Park, S.J. Porous Anodic Aluminum Oxide: Anodization and Templated Synthesis of Functional Nanostructures. *Chem. Rev.* **2014**, *114*, 7487–7556. [CrossRef] [PubMed]
38. Chahrour, K.M.; Ahmed, N.M.; Hashim, M.R.; Elfadill, N.G.; Maryam, W.; Ahmad, M.A.; Bououdina, M. Effects of the voltage and time of anodization on modulation of the pore dimensions of AAO films for nanomaterials synthesis. *Superlattices Microstruct.* **2015**, *88*, 489–500. [CrossRef]
39. Cheng, C.; Ng, K.Y.; Ngan, A.H.W. Quantitative characterization of acid concentration and temperature dependent self-ordering conditions of anodic porous alumina. *AIP Adv.* **2011**, *1*, 042113. [CrossRef]